Transient Natural Convection in a Vertical Cylinder

L. B. EVANS and R. C. REID

Massachusetts Institute of Technology, Cambridge, Massachusetts

E. M. DRAKE

Arthur D. Little, Inc., Cambridge, Massachusetts

An experimental and analytical study is reported of transient natural convection in a vertical cylinder. For the experiments a cylinder was partially filled with liquid and subjected to a uniform heat flux at the walls. Thermocouples were used to measure the unsteady temperature field within the liquid; dye tracers were used to study flow patterns. Parameters that were varied included the test liquid (water-glycerin mixtures), the liquid depth, and the wall heat flux. A range of Prandtl number from 2 to 8,000, L/D ratio from 1 to 3, and Grashof number from 10^3 to 10^{11} were studied, encompassing both laminar and turbulent flow regimes.

An analytical model was developed by dividing the system into three regions: a thin boundary layer rising along the heated walls, a mixing region at the top where the boundary layer discharges and mixes with the upper core fluid, and a main core region which slowly falls in plug flow. The temperature of the core fluid was assumed to vary in the vertical direction but not in the horizontal direction. Natural convection boundary-layer equations were modified to allow for a temperature variation at the outer edge of the boundary layer. The model may be used with a step-by-step computational procedure to predict the temperature distribution in the fluid as a function of time for an arbitrary set of conditions. Results computed by using the model were in good agreement with the experimental data.

The work described in this paper was directed toward obtaining an improved quantitative understanding of transient natural convection within an enclosed fluid This phenomenon, produced by heat transfer through the enclosure walls, is important in diverse engineering applications such as storage of cryogenic fluids, heating of buildings, start-up of a chemical reactor, and emergency cooling of nuclear fuel elements.

Although this paper is generally concerned with natural convective flows in large enclosures, where the boundary-layer flow does not occupy a major portion of system volume, some earlier work utilized similar analytical techniques in solving the problem of cooling turbine blades. In these studies, convective flow in narrow vertical tubes with a constant outside wall temperature was treated extensively by Lighthill (*7*) who employed an integral-momentum, boundary-layer analysis to describe various laminar and turbulent flow regimes. Ostrach and Thornton (*9*) also solved the particular case in which the tube wall temperature varied linearly with height.

More recently, stratification in cryogenic propellant storage tanks has stimulated a number of papers on the subject of convection in large enclosures. Much of this work has been summarized by Clark (*2*) who described a semiempirical model which has been applied extensively with minor variations to the problem. In the model, a flat-plate, natural convection, boundary-layer flow is assumed along the heated wall. The flow is discharged into an upper stratified region, and the bulk temperature below this region is assumed constant. The stratified region grows in depth as heat is added to the system. One of the serious limitations of this approach, as noted by Clark and others, is that the assumption of a constant bulk temperature is inaccurate except at very short times after the start of heating. Deficiencies in the model have generally been allowed for by various empirical techniques.

In a recent study, Tatom (*14*) measured transient axial temperature profiles in water for turbulent natural convection in a rectangular vertical cell. A number of combinations of side and bottom heat flux levels were investigated.

Data were used to determine two empirical coefficients (depending on modified Grashof number, side-to-bottom heat flux ratio, and cell height-to-width ratio) which then could be used to predict temperature profiles. Agreement between predicted and experimental mean temperature variation was found to be within 10%, although profiles could not be predicted accurately for the case of side-wall heating only.

Attempts to solve (by direct numerical techniques) the partial differential equations describing two-dimensional, bounded, natural convection energy and momentum transfer in enclosed fluids have been described by Hellums and Churchill (*6*), Wilkes and Churchill (*15*), and Barakat and Clark (*1*). Barakat overcame some of the numerical stability problems which were encountered in earlier work and was able to predict temperatures along the center line of the enclosure. However, at high Grashof numbers, he required large computation times, and, at the finest space grid used, convergence was not obtained in regions near the wall, in the corners, or a short distance below the surface. An important limitation on finite-difference solutions to this problem is that at high Grashof numbers the scale of actual boundary-layer widths and local eddy sizes in these regions may be considerably smaller than the smallest practical computation grid sizes.

PRESENT APPROACH

An experimental and analytical study was conducted with the aim of developing improved practical techniques for predicting transient, natural convection temperature fields in enclosed fluids. In the experimental portion of the study, a vertical cylinder, partially filled with liquid, was subjected to uniform side-wall heating. A range of Prandtl number from 2 to 8,000, L/D Ratio from 1 to 3, and Grashof numbers from 10^3 to 10^{11} was studied, encompassing both laminar and turbulent flow regimes.

Temperature measurements and dye tracer observations from thirty-four tests were used as guidelines in developing a system model. Since the actual natural convection flow exhibited boundary-layer characteristics, use of a modified boundary-layer analysis appeared justified. In an enclosed system, axial temperature gradients exist in the core region outside the boundary layer. The classical flat plate analysis assumes that fluid outside the boundary layer is isothermal. Therefore, the basic boundary-layer equations were rewritten to include terms allowing for an arbitrary axial temperature distribution at the outer edge of the layer. Other effects, such as starting transients and behavior at the start of the boundary layer, were investigated. In the analysis it was assumed that no heat or mass transfer occurred across the liquid-vapor interface, and this condition was also imposed on the experimental system.

EXPERIMENTAL INVESTIGATION

Apparatus

The experimental enclosure was an 8-in. diameter pyrex cylinder, held by tie rods between two gasketed end flanges as shown in Figure 1. A thin-film, transparent, electrically-conductive coating (E-C coating, Corning Glass Works) on the outside of the cylinder allowed controllable resistance heating of the walls while also permitting visual observation of flow tracers. The 2 ft. long cylinder was subdivided into three 8-in. cylindrical sections by circumferential silver bands deposited over the coating. Since each section could be heated independently, *L/D* ratios of 1, 2, and 3 could be studied by filling and heating one, two, or three sections. Test fluids were water, glycerin, and an 85 wt. % glycerin-water solution. Heating rates ranged from 20 to 2,000 B.t.u./(hr.) (sq. ft.). A free liquid surface, coated with a surfactant film to retard surface vaporization when necessary, was present in all tests. The bottom and top of the vessel were insulated, although the presence of the bottom flange prevented simulation of a true adiabatic boundary in this region.

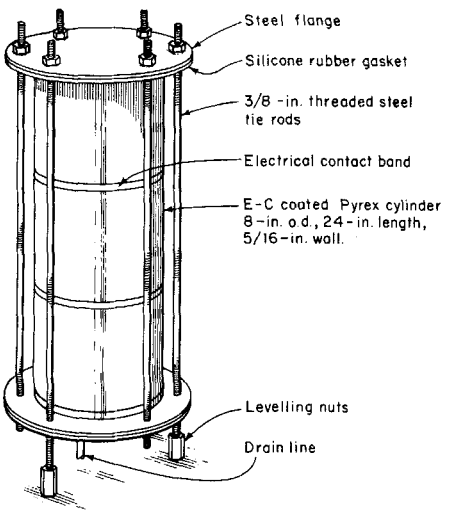

Fig. 1. Experimental enclosure.

Typical test durations ranged from ½ to 6 hr. Since the fluids were generally heated to a particular maximum temperature at which appreciable vaporization was detected, the longer test durations usually correspond to lower heating rates. During an experiment, temperature measurements were recorded, and, when desired, visual and/or photographic observations were made. Preliminary tests showed that there were no discernable azimuthal temperature gradients. Consequently, most of the temperature measurements were made over a single radial plane using thirty-eight, 3-mil thermocouples. The wires were threaded on a vertical support ladder positioned well behind the data plane to minimize any flow disturbance. Temperature readings were also obtained from one movable and two fixed thermocouples located outside the primary plane of measurement. These readings confirmed the fact that the temperature field had azimuthal symmetry.

Test Results

Temperature profile from a typical experimental run are shown in Figure 2. The increase in temperature, relative to the initial fluid temperature, is plotted as a function of dimensionless height at various times after the start of heating. The solid lines represent average fluid temperature; the dotted and

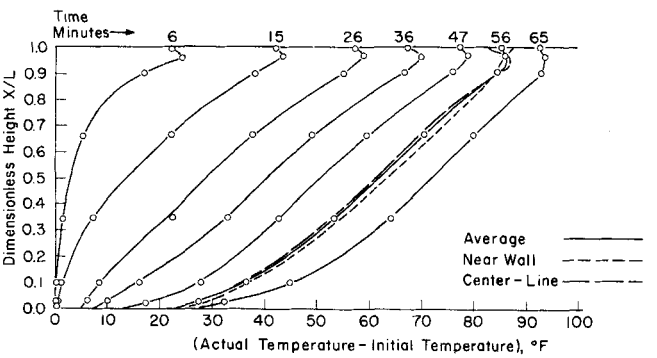

Fig. 2. Axial core temperature profiles for 85 wt.% glycerin-water, with L = 1.33 ft., D = 0.604 ft., and q_W = 500 B.t.u/(hr.)(sq. ft.).

dashed lines (shown only for 56 min.) indicate the temperature at the center line and at points only 0.05 in. from the wall. It is evident that there was very little radial temperature variation; this same phenomenon was observed in all of the experimental runs. A complete tabulation of the transient temperature measurements from all of the tests is available elsewhere (*3*). The dye tracer movements indicated in Figure 3

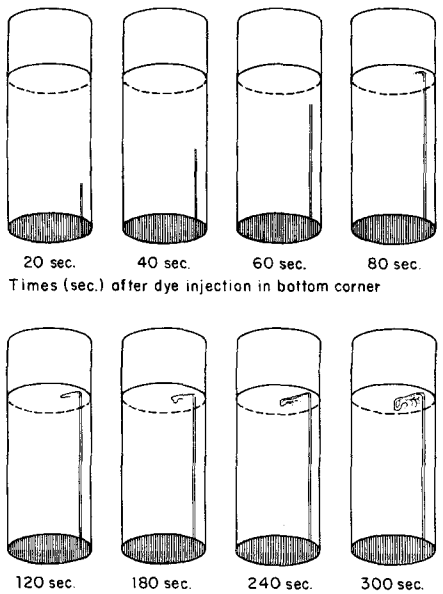

Fig. 3. Typical flow pattern observations (same test conditions as in Figure 2).

were sketched from a typical series of photographs. Analysis of such data from twenty-eight different runs covering a wide range of experimental conditions led to the following generalizations:

1. Side-wall heating results in a thin boundary-layer type of flow up the walls. For most tests, the boundary layer was so thin that it did not encompass the thermocouples located 0.05 in. from the wall. The maximum boundary-layer thickness occurred in glycerin tests near the top of the $L/D = 3$ configuration, but even then the thickness was less than 0.5 in.
2. Boundary-layer fluid is discharged radially inward just below the liquid surface. Although the mixing behavior was complex, and varied in detail from test to test, it was generally confined to about the upper 10% of the vessel.
3. Below the mixing region, radial temperature gradients in the fluid are small. The warmer fluid deposited near the top of the core settles gradually as cooler fluid from lower regions feeds the boundary layer. A plug-flow model appears reasonable for this region.
4. There is an initial transient period until the first warm fluid reaches the bottom of the vessel. After this period the axial core temperature variation becomes essentially linear with height. The value of the core temperature gradient increases slowly with time and varies with fluid properties, geometry, and wall heat flux level.
5. After the initial transient period the temperature rise at the midplane of the cylinder becomes equal to the bulk average temperature computed from an energy balance as

$$T_B - T_i = \frac{4}{\rho C_p D}\int_0^t q_w\, dt \qquad (1)$$

This is shown in Figure 4, where the midplane temperature rise is plotted vs. the bulk average temperature rise for all of the experiments including some results reported by Barakat (*1*) and Siefkes (*12*). The discrepancy at lower temperatures is due to the initial transient effect. At the start of heating the average fluid temperature begins to rise immediately, but the midplane core temperature does not begin to change until warm core fluid sinks to its level.

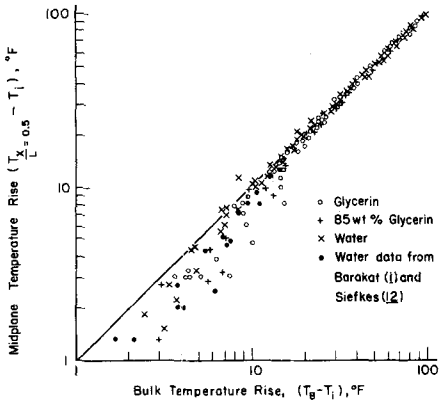

Fig. 4. Experimental midplane and bulk average temperature increase.

An indication of the complexity of the temperature profiles during the initial transient can be seen in Figures 5 and 6. The temperature rise at each axial position was normalized by dividing by the bulk average temperature rise and plotted vs. a dimensionless time parameter. If the fluid were perfectly mixed, the ratios would all be unity. The deviation from unity indicates the distribution of thermal energy within the system. This method of plotting satisfactorily accounts for the effects of L/D and wall heat flux. But, the data for water had to be plotted separately from the data for the two glycerin solutions.

Figures 5 and 6 may be used empirically to estimate the transient temperature behavior of any system similar to that used in this investigation. Figure 6 also includes some data reported by Barakat (*1*) and Siefkes (*12*). Segel's (*11*) data for the axial temperature distribution in a liquid hydrogen tank also is in accord with these results. In addition, all of the generalizations about the qualitative behavior of the system are consistent with the experimental observations of Schwind and Vliet (*10*) for transient natural convection in a rectangular cell.

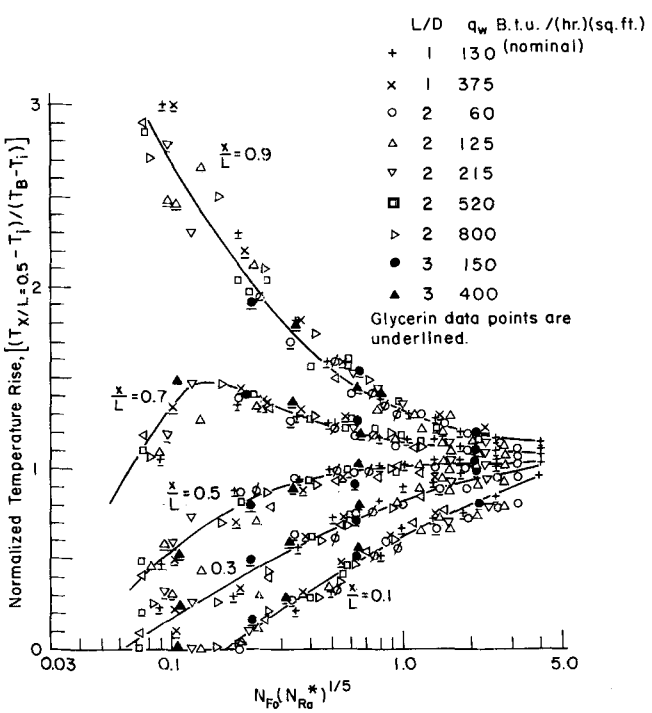

Fig. 5. Normalized transient temperature distribution for fluid in a vertical cylinder with constant wall heat flux (glycerin and 85% glycerin data).

At very high heat flux levels, a superimposed S shaped variation was observed in the axial temperature profile (Figure 14). This secondary effect may be due to a local instability in the boundary-layer flow (such as a transition to turbulence) which causes hot fluid to be injected into the core at an intermediate level below the surface. This effect has also been noted by others (*10, 14*).

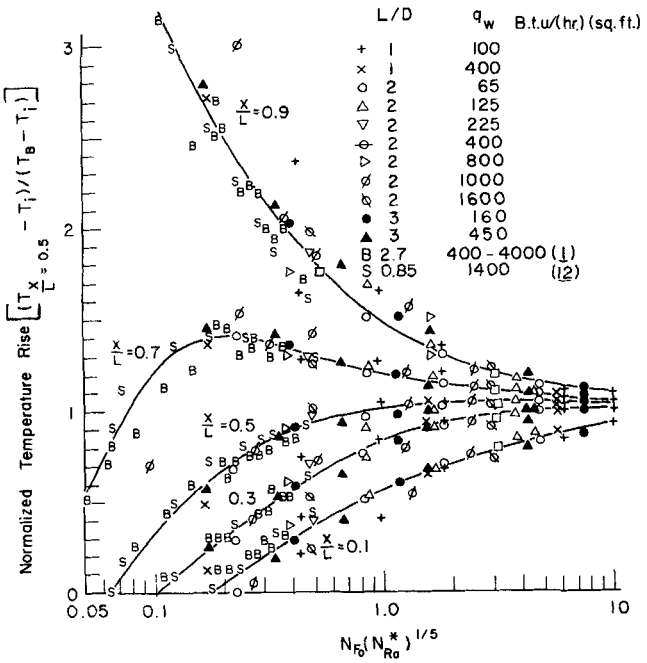

Fig. 6. Normalized transient temperature distributions for fluid in a vertical cylinder with constant wall heat flux (water data).

FORMULATION OF A MODEL

On the basis of the experimental observations, the system was modeled in terms of three regions: a mixing region at the top, a central core, and a boundary layer rising at the heated wall as shown in Figure 7. The equations describing each separate region will be presented and then combined into a model of the overall system.

Mixing Region

The hypothetical mixing region is considered to extend to a depth H and to be at uniform temperature T_m. An energy balance on the mixing region (with thermal energy referred to a datum temperature T_m) may be written as

$$\rho C_p \frac{\pi D^2}{4} H \frac{dT_m}{dt} = \rho C_p \pi D \int_0^{\delta_L} u_L (T_L - T_m)\, dy \quad (2)$$

The variables T_L, u_L, and δ_L are, respectively, the instantaneous temperature, vertical velocity, and thickness of the boundary-layer fluid where it enters the mixing region.

Central Core

It is assumed that the temperature T_c of the core fluid at any time is uniform in the radial direction but varies in the axial direction, and that the core fluid moves downward with plug flow velocity u_c. By integrating the fluid velocity across a horizontal plane at the position where it enters the mixing region, and by noting that there is no accumulation of fluid in the mixing region, the following result is obtained:

$$\pi D \int_0^{\delta_L} u_L dy - \frac{\pi}{4} (D - 2\delta_L)^2 u_c \Big|_{x=L} = 0 \quad (3)$$

By neglecting the fraction of fluid lost from the core by entrainment into the boundary layer and by noting that $\delta_L << D$, the instantaneous velocity of the core fluid at any position may be satisfactorily approximated by

$$u_c = \frac{4}{D} \int_0^{\delta_L} u_L dy \quad (4)$$

A thermal energy balance on a differential element of the core fluid yields

$$u_c \frac{\partial T_c}{\partial x} = \frac{\partial T_c}{\partial t} \quad (5)$$

This derivation assumes that axial conduction is negligible and that there is no heat transfer directly from the boundary layer to the core fluid.

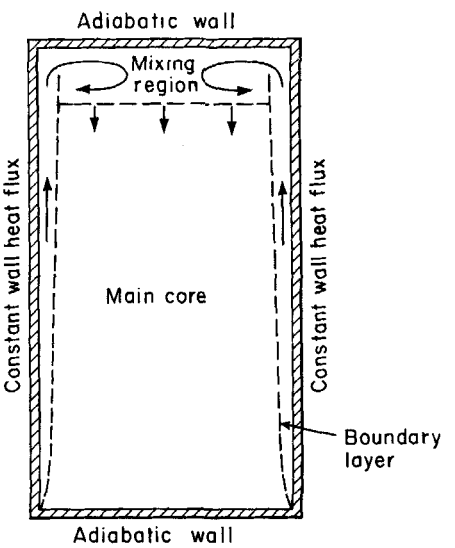

Fig. 7. Model for natural convection within a vertical cylinder for constant wall heat flux.

Boundary Layer

Since the boundary-layer thickness is small relative to the cylinder radius, the wall may be treated as a vertical flat plate. The analysis is complicated, however, by the fact that the temperature T_∞ of the fluid outside the boundary layer is not constant but varies with vertical position. For use in the overall model T_∞ is synonymous with the core temperature. A detailed analysis of free convection from a vertical plate to a nonisothermal fluid is described elsewhere (3); only the results essential to the overall model will be summarized here.

The integrated forms of the momentum and energy equations for steady state boundary-layer flow are

$$\frac{\partial}{\partial x} \int_0^{\infty} u^2 dy = \beta g \int_0^{\infty} (T - T_\infty)\, dy - \frac{\tau_w}{\rho} \quad (6)$$

$$\frac{\partial}{\partial x}\int_0^\infty u(T-T_\infty)dy = \frac{q_w}{\rho C_p} - \int_0^\infty u\frac{\partial T_\infty}{\partial x}dy \quad (7)$$

The only difference between the above equations and those used successfully by other investigators (8, 13) for the case of T_∞ constant is the occurrence of the last term in the energy equation. If the surrounding fluid is isothermal, this term is zero.

The solution of these equations for laminar flow is outlined below; the corresponding development for turbulent flow is given in the appendix. For laminar flow the following functional forms are assumed for the velocity and temperature profiles within the boundary layer ($0 \leq y \leq \delta$):

$$u = \omega\left(\frac{y}{\delta}\right)\left(1-\frac{y}{\delta}\right)^2 \quad (8)$$

$$T - T_\infty = \frac{q_w}{2k}\delta\left(1-\frac{y}{\delta}\right)^2 \quad (9)$$

Outside the boundary layer ($y > \delta$), $u = 0$ and $T = T_\infty$. The wall shear stress is given by the familiar expression for a Newtonian fluid:

$$\tau_w = -\mu\left.\frac{\partial u}{\partial y}\right|_{y=0} \quad (10)$$

When Equations (8), (9), and (10) are substituted into (6) and (7), a pair of simultaneous ordinary differential equations are obtained which define the unknown functions $\delta(x)$ and $\omega(x)$. It is convenient to define new dimensionless variables: $X = Cx$, $M^* = \omega^2\delta/C\nu^2C_M$, $E^* = \omega\delta^2C/C_E\nu$, and $\theta'_\infty = \left(\frac{k}{q_w}\right)\frac{dT_\infty}{dX}$, where

$$C = \left(\frac{g\beta q_w}{k\nu^2}\right)^{1/4} \quad (11)$$

$$C_M = \left(\frac{60}{N_{Pr}}\right)^{4/5}\left(\frac{10}{4/5+N_{Pr}}\right)^{3/5} \quad (12)$$

$$C_E = \frac{60}{N_{Pr}} \quad (13)$$

In terms of these new dimensionless variables the pair of simultaneous ordinary differential equations are

$$\frac{dM^*}{dX} = \left[\frac{7}{5}+\frac{7}{4}N_{Pr}\right]\frac{E^{*4/3}}{M^{*2/3}} - \frac{7}{4}N_{Pr}\frac{M^*}{E^*} \quad (14)$$

$$\frac{dE^*}{dX} = 1 - 5\left(\frac{60}{N_{Pr}}\right)^{3/5}\left(\frac{10}{4/5+N_{Pr}}\right)^{1/5}(E^*M^*)^{1/3}\theta'_\infty \quad (15)$$

with the initial conditions: at $X = 0$, $M^* = 0$ and $E^* = 0$. These new variables have the physical significance that M^* and E^* are proportional to the convective transport, respectively, of momentum and thermal energy (relative to the fluid at infinity) in the boundary layer. The original variables δ and ω are related to M^* and E^* by

$$\delta = \frac{1}{C}\left[\frac{C_E^2E^{*2}}{C_M M^*}\right]^{1/3} \quad (16)$$

$$\omega = C\nu\left[\frac{C_M^2 M^{*2}}{C_E E^*}\right]^{1/3} \quad (17)$$

The dimensionless distance X is simply the one-fourth power of the local modified Grashof number N_{Gr}^*

For the case of a constant core temperature fluid $\theta'_\infty = 0$, it can be verified that the solution is $M_o^* = X^{7/5}$ and $E_o^* = X$ which agrees with the work of Sparrow (13). For any specified but arbitrary variation of θ'_∞ with X, Equations (14) and (15) may be integrated numerically.

In this study, numerical solutions were obtained for the important case of θ'_∞ = constant, corresponding to the experimentally observed linear axial temperature distribution. The results are shown in Figures 8 and 9 for the laminar and turbulent cases, respectively, and for a range of N_{Pr} and θ'_∞ encountered in the experimental phase of the study. The details of the numerical solution are described elsewhere (3).

When the temperature at infinity is constant, both the boundary-layer thermal energy and momentum (as well as velocity and boundary-layer thickness) increase with distance up the wall. If, however, a positive core temperature gradient is present, the boundary-layer parameters E^* and M^* reach asymptotic limiting values. The physical interpretation of this phenomenon is that eventually the boundary layer grows so large that all of the wall heat flux is required to keep the average temperature level of the boundary-layer fluid increasing at the same rate as that of the core fluid. Consequently, there is no thermal energy available for additional growth or acceleration of the boundary-layer fluid.

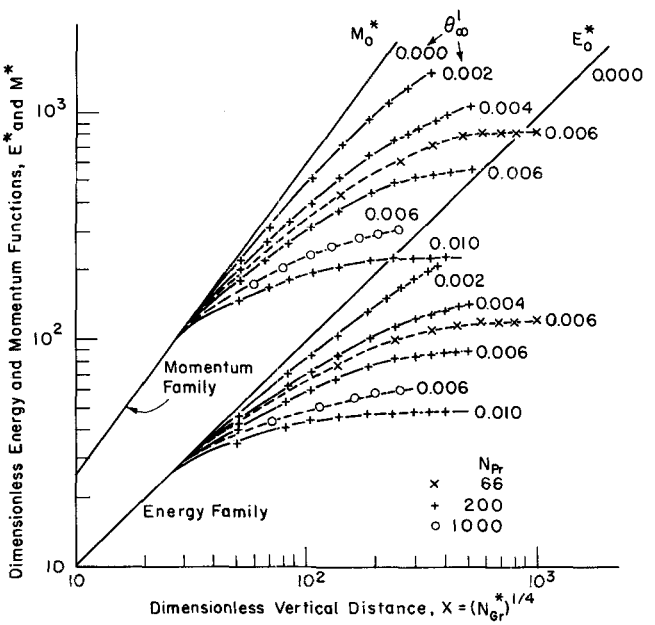

Fig. 8. Dimensionless boundary-layer energy and momentum functions: laminar model with constant core temperature gradient.

The limiting asymptotic values E_a^* and M_a^* may be found by setting the derivatives in Equations (14) and (15) equal to zero and by solving the equations simultaneously to obtain

$$E_a^* = \frac{0.582}{N_{Pr}^{1/4}(\theta'_\infty)^{5/4}} \quad (18)$$

$$M_a^* = \frac{0.471}{N_{Pr}^{7/20}(\theta'_\infty)^{7/4}}\left[\frac{11/5+N_{Pr}}{N_{Pr}}\right]^{3/5} \quad (19)$$

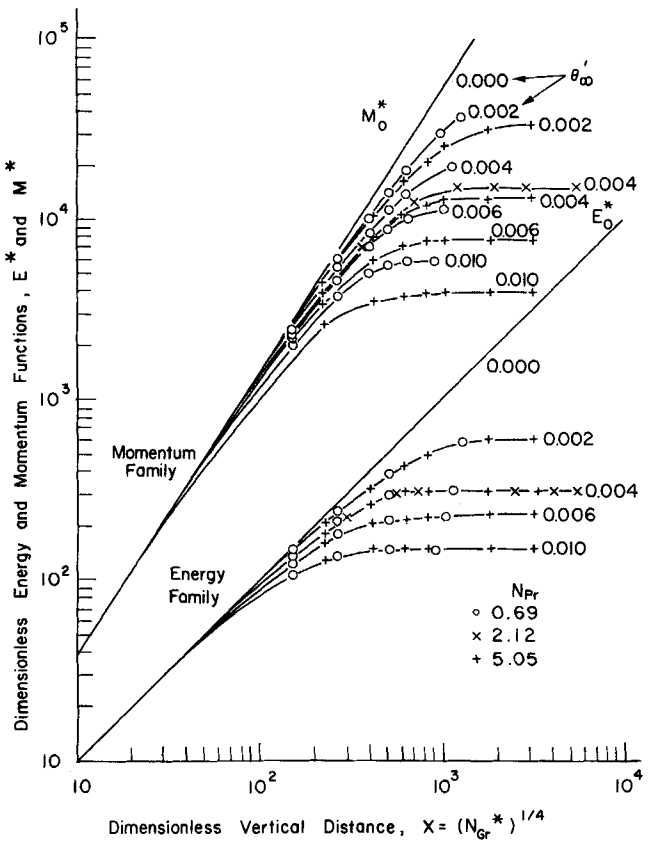

Fig. 9. Dimensionless boundary-layer energy and momentum functions: turbulent model with specified constant core temperature gradient.

The overall model may be used to predict transient temperature profiles as follows. Initially, at time $t = 0$, the temperature T_m of the mixing region and the core temperature distribution $T_c(x)$ are equal to the initial bulk fluid temperature T_o. The integrals I_1 and I_2 defined above are initially zero. The continuous core temperature distribution is represented numerically by discrete values of T_c at $x = 0, \Delta x, 2\Delta x, \ldots, L - H$. Equations (2), (4), and (5) are solved by a step-by-step procedure to advance the calculation from a time t to a new time $t + \Delta t$ with the condition that $T_c(L - H) = T_m$. Then the new core temperature distribution at the new time level is used (in dimensionless form) to solve the boundary-layer Equations (14) and (15) and determine the values of the integrals I_1 and I_2 at the new time level. This procedure can be applied iteratively to predict the transient bulk temperature distribution for any specified set of experimental conditions.

The only parameter in the model which may be adjusted arbitrarily to force agreement with experimental data is the depth H of the mixing region. Analysis of all of the data of this investigation indicated that the mixing region comprised about 10% of the total depth for both laminar and turbulent conditions.

The iterative procedure was used to calculate the core temperature distribution corresponding to a particular set of experimental conditions. The results are shown in Figure 10. It can be seen that the calculated results are in good quantitative agreement with the experimental data. After a brief initial transient period required for the first warm fluid to reach the bottom of the cylinder, the core temperature distribution became linear as was observed experimentally.

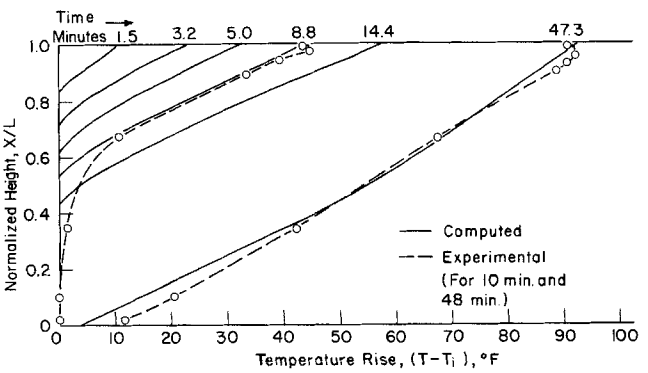

Fig. 10. Step-by-step computer solution for initial period transient axial temperature distributions [100% glycerin, $L = 1.33$ ft., $D = 0.604$ ft., $q_W = 500$ B.t.u./(hr.)(sq. ft.)].

Overall System

The separate equations to describe the behavior of the mixing region, central core, and boundary layer may be combined and solved simultaneously to predict the overall behavior of the system.

It is assumed that the behavior of the boundary layer during transient heating of the enclosed fluid can be described at any instant in time by the solution of the steady state Equations (14) and (15) with the instantaneous values of $T_\infty(x)$. This quasi steady state approximation is justified by the fact that the time required for the boundary layer to respond to changes in its forcing variables is much smaller than that required for changes to occur throughout the bulk fluid. For example, when a heat flux is first imposed upon an initially isothermal, quiescent fluid, the time required to establish a steady state boundary layer flow is small. (Typical durations for this starting transient are 1 to 5 sec.) In contrast, the time required for significant changes to take place in the bulk fluid is on the order of a few minutes.

The integrals required in Equations (2) and (4) can be obtained directly from the solution to the boundary-layer equations by using the following relations:

$$I_1 = \int_0^{\delta_L} u_L dy = \frac{\nu}{12} (C_M C_E M_L^* E_L^*)^{1/3} \qquad (20)$$

$$I_2 = \int_0^{\delta_L} u_L (T_L - T_m) dy = \frac{q_w}{C\rho C_p} E_L^* \qquad (21)$$

In the above M_L^* and E_L^* are the solutions to (14) and (15) at a dimensionless distance corresponding to $x = L$.

Analytical Solution Valid after Initial Transient

A specialized analytical solution to the model equations was obtained by assuming that the core temperature distribution was linear. The experimental observations indicated that these conditions held after the initial period of time required for the first warm fluid to reach the bottom of the tank. The zero point on the temperature scale is chosen to be the instantaneous value of the temperature of fluid at the bottom of the vessel. With the above assumptions, the rate of change of the dimensionless core temperature gradient is

$$\frac{d\theta'_\infty}{dt} = \frac{k}{q_w(L - H)} \frac{dT_m}{dt} \qquad (22)$$

By substituting Equation (2) for dT_m/dt and (21) for the integral in that equation, the following result is obtained:

$$\frac{d\theta'_\infty}{dt} = \frac{4\alpha}{H(L-H)DC} E_L^* \qquad (23)$$

Once again, the quasi steady state approximation has been made. Since E_L^* is a known function of X_L, N_{Pr}, and θ'_∞, the equation could be integrated at least numerically to give θ'_∞ as a function of time. In most cases of practical importance, however, the boundary layer will have achieved its limiting asymptotic behavior at the top of the vessel with $E_L^* = E_a^*$. By substituting (18) into (23) and integrating, the following result is obtained:

$$\theta'_\infty = A_1 \left[\frac{\alpha t}{DL}\right]^{4/9} N_{Ra^*}{}^{-1/9} \qquad (24)$$

The constant A_1 contains the empirical parameter H/L and is given by

$$A_1 = \left[\frac{(9)(0.582)}{(1-H/L)(H/L)}\right]^{4/9} \qquad (25)$$

To test the validity of this approximate analytical solution, experimental values of θ'_∞ were plotted against $N_{Fo}{}^{4/9} N_{Ra}{}^{*-1/9}$ in Figure 11 for glycerin and in Figure 12 for water. The results show remarkable agreement; all of the data fall on a straight line corresponding to a constant $A_1 = 4.0$. The data for water agree well with the laminar model, even though on the basis of $N_{Gr}^* > 10^{11}$ they might have been expected to be turbulent.

The equation developed for turbulent flow, analogous to (24), was

$$\theta'_\infty = B_1 \left[\frac{\alpha t}{LD}\right]^{8/15} N_{Pr}{}^{7/45} N_{Ra}{}^{*-2/15} \qquad (26)$$

with

$$B_1 = \left[\frac{(15/2)(2.48)}{(1-H/L)(H/L)}\right]^{8/15} \qquad (27)$$

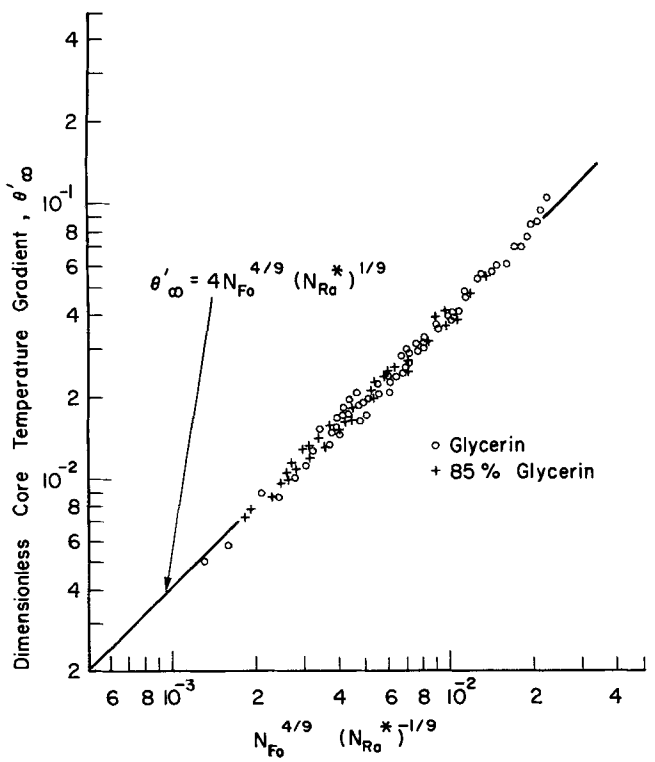

Fig. 11. Axial core temperature gradient for comparison of glycerin and 85% glycerin data with laminar model.

This was tested by plotting θ'_∞ vs. $N_{Fo}{}^{8/15} N_{Pr}{}^{7/45} N_{Ra}{}^{*-2/15}$ for all of the data in Figure 12. The nominally laminar data (corresponding to $N_{Gr}^* < 10^{11}$) were not correlated, as would be expected. If the usual criterion for transition to turbulent natural convection is considered, then most of the water data should have been for turbulent conditions. However, the boundary-layer analysis indicated that the presence of a core temperature gradient reduces and limits the boundary-layer energy and momentum. Therefore, one might anticipate that this effect would also delay transition to turbulence.

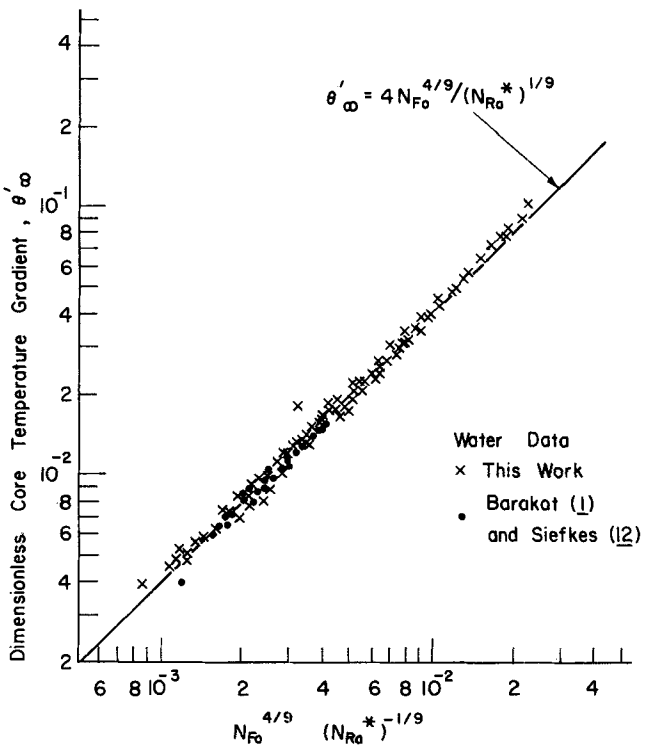

Fig. 12. Axial core temperature gradient for comparison of water data with laminar model.

The value of E^* might be a better criterion for transition to turbulence than the modified Grashof number. For a flat plate in an isothermal fluid, it has been reported (*11*) that transition occurs at $N_{Gr}^* \approx 10^{11}$ which corresponds to $E^* \approx 500$, since $E^* = N_{Gr}{}^{*1/4}$ for this case. Hence, in the presence of a core temperature gradient it seems plausible to expect that transition would occur whenever E^* became greater than 500.

On this basis, the turbulent transition would not occur for those data marked *nominally turbulent* in Figure 13. The remaining data which should be turbulent on the basis of an E^* criterion fit the analytical correlation quite well with a constant $B_1 = 11.5$.

Experimental observations in this and other work (*10, 14*) also indicate that the boundary-layer energy limitation and the delay of turbulent transition are real effects in the physical system.

Values of H/L equal to 0.35 and 0.25, respectively, are required by Equations (25) and (27) to predict the experimentally determined values $A_1 = 4.0$ and $B_1 = 11.5$. Observation of the flow patterns indicated, however, that fluid mixing was confined to about the upper 10% of the vessel. The fact that a larger value of H/L is required to correlate the core temperature gradient data may be attributed to several factors: a highly simplified

model of the system was chosen, solutions to the integrated form of the boundary-layer equations are not exact, and steady state solutions to the boundary-layer equations were applied under quasi steady state conditions. Nonetheless, the excellent correlation of the data indicates that the form of the analytical solution is correct. All that would be expected from a more rigorous analysis would be to refine the a priori prediction of the constants A_1 and B_1.

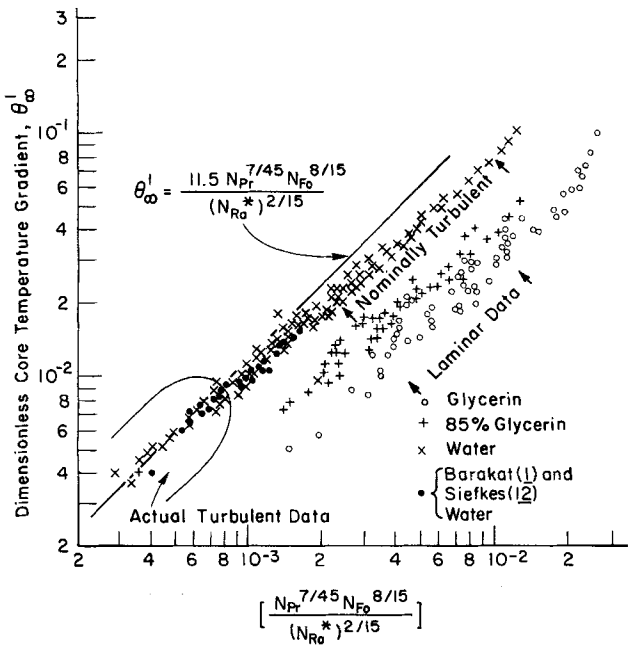

Fig. 13. Axial core temperature gradient for comparison of all data with turbulent model.

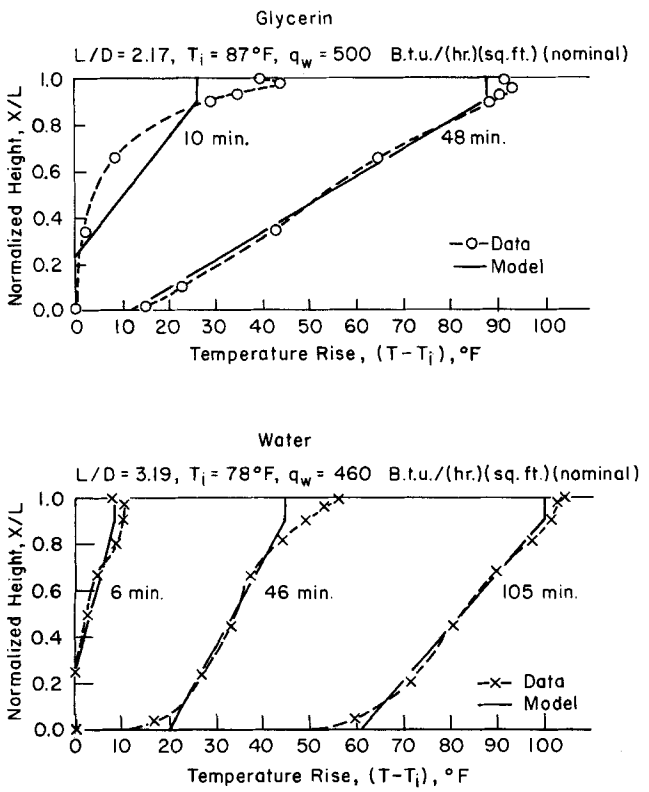

Fig. 14. Limiting boundary-layer energy model, comparison between predicted and observed axial core temperature profiles.

By assuming that the core temperature distribution is linear with the midplane temperature equal to the mixed-mean fluid temperature, the transient temperature distribution may be predicted by using Equations (24) or (26). Figure 14 shows a comparison between temperature profiles predicted in this manner and actual profiles measured for equivalent conditions. Agreement is good except during the initial transient period. Before the first warm fluid reaches the bottom of the core, the core temperature profile is not linear, and the use of a mixed-mean temperature as the midpoint temperature is not valid.

SUMMARY AND CONCLUSIONS

An extensive experimental study was made of transient natural convection temperature fields and circulation patterns within a vertical cylinder subjected to a uniform wall heat flux. The experiments showed that the system was characterized by a very thin boundary layer rising at the wall, a rapid turning of the boundary layer into the central core region just below the free liquid surface, excellent radial mixing of the warm boundary-layer fluid near the surface, and gradual plug-flow sinking of the radially mixed fluid as still warmer fluid displaces it and cool fluid is fed to the boundary layer from below.

A mathematical model was developed by dividing the system into three regions: a boundary layer, a mixing region at the top, and a central core that falls slowly in plug flow. A new boundary-layer analysis was employed which allows for temperature variation at the outer edge of the boundary layer. This model of the system can be used with a step-by-step numerical technique to calculate temperature profiles in enclosed fluid subjected to wall heating.

After an initial transient period, defined as the interval required for the first warm fluid to sink to the bottom of the vessel, the core temperature becomes linear with a gradient that increases with time. The core temperature gradient can be predicted from Equations (24) or (26) which are based upon a simplified analytical solution to the model equations and were confirmed by all of the experimental data. The core temperature at the midplane of the cylinder becomes essentially equal to the mixed-mean fluid temperature after the initial transient period. By assuming that the core temperature distribution is linear, approximate temperature profiles can be computed which, after the initial transient, predict the experimental behavior.

The presence of a positive axial temperature gradient limits the energy in the boundary-layer flow and delays the transition to turbulence. It is proposed that in an enclosed system the transition to turbulence will occur whenever the dimensionless boundary-layer energy E^* exceeds about 500. In the absence of a core temperature gradient this is equivalent to the commonly accepted criterion of $N_{Gr}^* > 10^{11}$ for a vertical plate.

ACKNOWLEDGMENT

Financial support for this work was provided by the National Science Foundation (grant GK-243) and by the Sloan Basic Research Program. E. M. Drake received fellowship support from the National Science Foundation. Use of the facilities of the Massachusetts Institute of Technology Computation Center is gratefully acknowledged.

The authors wish also to thank Professor Kenneth A. Smith for providing many helpful suggestions including the use of the integral momentum method.

NOTATION

A_1 = empirical coefficient defined by Equation (25)
B_1 = empirical coefficient defined by Equation (27)
C = dimensional factor $[g\beta q_w/k\nu^2]^{1/4}$
C_E = energy coefficient, dimensionless
C_M = momentum coefficient, dimensionless
C_p = fluid specific heat capacity, B.t.u./(lb.)(°F.)
D = diameter, ft.
E^* = normalized dimensionless boundary-layer energy parameter
g = acceleration of gravity, ft./(hr.)^2
H = mixing region depth, ft.
k = thermal conductivity, B.t.u./(hr.)(ft.)(°F.)
L = total height of fluid, ft.
L/D = aspect ratio
M^* = normalized dimensionless boundary-layer momentum parameter
q_w = heat flux at wall, B.t.u./(hr.)(sq.ft.)
t = time, hr.
T = temperature, °F.
T_B = bulk mean temperature, °F.
u = velocity in x-direction, ft./hr.
x = Cartesian coordinate (opposed to direction of gravity), ft.
X = dimensionless x coordinate
y = Cartesian coordinate, ft.

Dimensionless Groups

N_{Fo} = Fourier number, $\alpha t/LD$
N_{Gr} = Grashof number, $g\beta(T_w - T_o)L^3/\nu^2$
N_{Gr}^* = modified Grashof number, $N_{Gr}^* = (N_{Gr})(N_{Nu}) = g\beta q_w L^4/k\nu^2$
N_{Nu} = Nusselt number, hL/k
N_{Pr} = Prandtl number, ν/α
N_{Ra} = Rayleigh number, $(N_{Gr})(N_{Pr})$
N_{Ra}^* = modified Rayleigh number, $(N_{Gr}^*)(N_{Pr})$

Greek Letters

α = thermal diffusivity, sq.ft./hr.
β = coefficient of thermal expansion, $(°F.)^{-1}$
δ = boundary-layer width, ft.
θ_x = dimensionless core temperature (kCT_x/q_w)
θ'_∞ = dimensionless core temperature gradient, $d\theta_x/dX$
ν = kinematic viscosity, sq.ft./hr.
ρ = density, lb./cu.ft.
τ_w = shear stress at wall, lb./(ft.)(hr.)^2
ω = boundary layer velocity scale, ft./hr.

Subscripts

a = asymptotic value
c = core
i = initial
L = at $x = L$, boundary-layer discharge point
m = mixing region, inlet to top of core region
o = isothermal core fluid
∞ = outside boundary layer, at $y = \infty$

LITERATURE CITED

1. Barakat, H. Z., and J. A. Clark, "Proceedings Third International Heat Transfer Conference," Vol. 2, p. 152 (1966).
2. Clark, J. A., *Intern. Adv. Cryo. Eng.*, **10**, 259 (1964).
3. Drake, E. M., Sc.D. thesis, Mass. Inst. Technol., Cambridge (1966).
4. Eckert, E. R. G., and T. W. Jackson, *Natl. Advisory Comm. Aeronaut. Rept. 1015* (1950).
5. Evans, L. B., and N. E. Stefany, *Chem. Eng. Progr. Symposium Ser. No. 64*, **62**, 209 (1966).
6. Hellums J. D., and S. W. Churchill, *AIChE J.*, **8**, 690 (1962).
7. Lighthill, M. J., *Quart. J. Mech. Appl. Math.*, **6**, 398 (1953).
8. Ostrach, Simon, *Natl. Advisory Comm. Aeronaut. Tech. Rept. 1111* (1953).
9. ———, and P. R. Thornton, *Trans. Am. Soc. Mech. Engrs.*, **80**, 363 (1958).
10. Schwind, R. G., and G. C. Vliet, "Proceedings of the 1964 Heat Transfer and Fluid Mechanics Institute," Vol. 51, p. 52, Stanford Univ. Press, Palo Alto, Calif. (1964).
11. Segel, M. P., *Intern. Adv. Cryo. Eng.*, **10**, 308 (1964).
12. Siefkes, Donald, S. B. thesis, Mass. Inst. Technol., Cambridge (1964).
13. Sparrow, E. M., and J. L. Gregg, *Trans. Am. Soc. Mech. Engrs. J. Heat Transfer*, **78**, 435 (1956).
14. Tatom, J. W., and W. O Carlson, "Proceedings Third International Heat Transfer Conference," Vol. 2, p. 163 (Aug. 9, 1966).
15. Wilkes, J. O., and S. W. Churchill, *AIChE J.*, **12**, 161 (1966).

Manuscript received February 13, 1967; revision received July 3, 1967; paper accepted July 5, 1967. Paper presented at AIChE Houston Meeting.

APPENDIX: ANALYSIS FOR TURBULENT BOUNDARY LAYER

The analysis for a turbulent boundary layer proceeds exactly as for the laminar case, except that Equations (8) through (10) become

$$u = \omega \left(\frac{y}{\delta}\right)^{1/7} \left(1 - \frac{y}{\delta}\right)^4 \tag{A1}$$

$$T - T_\infty = (T_w - T_\infty)\left[1 - \left(\frac{y}{\delta}\right)^{1/7}\right] \tag{A2}$$

$$\tau_w = 0.0225\,\omega^2\rho\left(\frac{\nu}{\omega\delta}\right)^{1/4} \tag{A3}$$

The only dimensionless variable defined differently for the turbulent case is

$$M^* = \frac{\omega^{1/4}\,\delta^{5/4}\,C}{C_M\,\nu^{1/4}} \tag{A4}$$

For the turbulent case Equations (12) through (18) become

$$C_E = \frac{0.61425}{N_{Pr}^{2/3}} \tag{A5}$$

$$C_M = \left[\frac{3.44\,N_{Pr}^{1/3}}{\frac{11}{7} + 0.702\,N_{Pr}^{2/3}}\right]^{9/14} C_E^{13/14} \tag{A6}$$

$$\frac{dE^*}{dX} = 1 - 0.14635\,N_{Pr}C_E^{2/7}\,(C_M C_E E^* M^*)^{4/9}\,\theta_\infty' \tag{A7}$$

$$\frac{dM^*}{dX} = \left[\frac{11}{7} + 0.702\,N_{Pr}^{2/3}\right]\frac{E^{*13/9}}{M^{*5/9}} - 0.702\,N_{Pr}^{2/3}\frac{M^*}{E^*} \tag{A8}$$

$$\delta = \frac{(C_M M^*)^{4/3}}{C(C_E E^*)^{1/3}} \tag{A9}$$

$$\omega = \frac{C\,\nu\,(C_E E^*)^{5/3}}{(C_M M^*)^{8/3}} \tag{A10}$$

$$E_a^* = 2.48\,N_{Pr}^{1/24}\,\theta_\infty'^{-7/8} \tag{A11}$$